Abstract for 37th IWWWFB, Giardini Naxos, Italy - April 10-13, 2022

Water wave interaction with an annular metamaterial cylinder

S. Zheng[a], R. Porter[b], H. Liang[c], D. Greaves[a]

a School of Engineering, Computing & Mathematics, University of Plymouth, Drake Circus, Plymouth PL4 8AA, United Kingdom

siming.zheng@plymouth.ac.uk; deborah.greaves@plymouth.ac.uk

b School of Mathematics, University of Bristol, Woodland Road, Bristol BS8 1UG, United Kingdom

richard.porter@bristol.ac.uk

c Technology Centre for Offshore and Marine, Singapore (TCOMS), 118411, Singapore

liang_hui@tcoms.sg

Highlights

We study water wave scattering by an annular metamaterial cylinder, which is composed of a series of radially aligned closely spaced plates, with both analytical and numerical methods.

- We find there can be hardly any back scattering for a wide range of wave frequencies;
- The resonant frequencies are predicted, around which the near non-back-scattering generally happens;
- We observe and theoretically prove that there is not any scattered wave contribution at the center point of the annular metamaterial cylinder.

1 Mathematical model

An annular metamaterial cylinder subjected to unidirectional regular waves in water of finite depth h is considered. The annular cylinder with its inner and outer radii denoted as $R_{\rm i}$ and R, respectively, is composed of a periodic array of infinitely–thin vertical plates aligned with the radial direction. A global Cartesian coordinate system $Oxyz$ is chosen with the mean free–surface coinciding with the (x, y)–plane, Oz placed at the axis of the cylinder pointing vertically upwards, and Ox coinciding with the incident wave direction. Hence the fluid bottom is at $z = -h$. Moreover, a cylindrical coordinate system, $Or\theta z$, are chosen for the purpose of convenience of mathematical expression. Fluid is allowed to flow in gaps between adjacent plates and waves are supported by the free surface. The effect of these plates of annular cylinder allows waves to propagate in the Or–direction only. The fluid domain can be divided into an annular domain, which fills the annular metamaterial cylinder, an exterior domain, representing the fluid domain outside the metamaterial cylinder extending towards infinity horizontally, and a inner region.

We assume that all amplitudes are small enough that linear theory applies and we make the usual assumptions that the fluid is inviscid, incompressible and its motion is irrotational. We denote the fluid velocity potential by $\Phi(x, y, z, t)$. It is further assumed that all motion is time–harmonic with angular frequency ω. Thus, we can write

$$\Phi(x, y, z, t) = \mathrm{Re}\{\phi(x, y, z)\mathrm{e}^{-\mathrm{i}\omega t}\}, \tag{1}$$

where Re denotes the real part. Thus ϕ is the spatial velocity potential which is independent of time, i.e., t. i is the imaginary unit. The spatial velocity potential satisfies Laplace equation,

$$\bigtriangledown^2 \phi = 0 \quad \text{in the water}, \tag{2}$$

and the boundary conditions at sea bed and free surface.

Within the fluid in the annular cylinder, Eq. (2) also holds although it is confined to narrow disconnected domains bounded by thin plates aligned with the radial direction of the $Or\theta z$ coordinate. Writing Eq. (2) in coordinate $Or\theta z$ and imposing the boundary conditions on the channel walls, it shows that the field within the whole of the annular cylinder is governed by an effective medium governing equation involving the reduced Laplacian:

$$\left(\frac{\partial^2}{\partial r^2} + \frac{1}{r}\frac{\partial}{\partial r} + \frac{\partial^2}{\partial z^2}\right)\phi = 0. \tag{3}$$

See also [1, 5] who employed the same models. Eq. (3) conservation of mass for an irrotational flow in which the motion perpendicular to the plates is inhibited.

Expressions of spatial velocity potential in different domains.–The spatial velocity potential in the exterior domain can be expressed as

$$\phi_{ext} = \phi_I + Z_0(z)\sum_{n=0}^{\infty} A_n H_n(kr)\cos(n\theta), \tag{4}$$

where ϕ_I represents the velocity potential of incident waves. The second term denotes the components contributed by the waves scattered from the cylinder. A_n are the unknown coefficients to be determined; H_n denotes the Hankel function of the first kind of order n; $Z_0(z) = \frac{\cosh[k(z+h)]}{\cosh(kh)}$; k is associated with propagating waves, and it is the positive real root of the dispersion relation for the exterior domain

$$\omega^2 = gk\tanh(kh), \tag{5}$$

where g denotes the acceleration due to gravity.

For the plane incident waves with amplitude A, angular frequency ω and wave direction $\beta = 0$, ϕ_I can be expressed in the coordinate systems of $Oxyz$ and $Or\theta z$, respectively, as

$$\phi_I = -\frac{\mathrm{i}gA}{\omega}\mathrm{e}^{\mathrm{i}kx}Z_0(z) = -\frac{\mathrm{i}gA}{\omega}Z_0(z)\sum_{n=0}^{\infty}\epsilon_n\mathrm{i}^n J_n(kr)\cos(n\theta), \tag{6}$$

where J_n is the Bessel function of the first kind of order n. ϵ_0=1, and ϵ_n=2 for $n > 0$.

The spatial velocity potentials in the interior and annular domains can be expressed as

$$\phi_{int}(r,\theta,z) = Z_0(z)\sum_{n=0}^{\infty}B_n J_n(kr)\cos(n\theta), \tag{7}$$

and

$$\phi_{ann}(r,\theta,z) = Z_0(z)\sum_{n=0}^{\infty}[C_n J_0(kr) + D_n Y_0(kr)]\cos(n\theta), \tag{8}$$

respectively, in which B_n, C_n, and D_n are unknown coefficients to be determined; Y_0 denotes the Bessel function of the second kind (also known as the Neumann function) of order 0.

The unknown coefficients, A_n, B_n, C_n, and D_n, in the expressions of the velocity potentials can be calculated by satisfying the continuity of the field in terms of pressure and flux across the interfaces of the annular, exterior, and interior domains, resulting in four sets of equations, i.e.,

$$\begin{pmatrix} J_n(kR_\mathrm{i}) & 0 & -J_0(kR_\mathrm{i}) & -Y_0(kR_\mathrm{i}) \\ J_n'(kR_\mathrm{i}) & 0 & -J_0'(kR_\mathrm{i}) & -Y_0'(kR_\mathrm{i}) \\ 0 & H_n(kR) & -J_0(kR) & -Y_0(kR) \\ 0 & H_n'(kR) & -J_0'(kR) & -Y_0'(kR) \end{pmatrix} \begin{pmatrix} A_n \\ B_n \\ C_n \\ D_n \end{pmatrix} = \frac{\mathrm{i}gA}{\omega}\epsilon_n\mathrm{i}^n \begin{pmatrix} 0 \\ 0 \\ J_n(kR) \\ J_n'(kR) \end{pmatrix}, \tag{9}$$

for the four unknown coefficients.

Wave elevation and the far-field scattering amplitude.–The wave elevation can be expressed as

$$\eta(r,\theta) = \frac{\mathrm{i}\omega}{g}\phi|_{z=0}. \tag{10}$$

The far–field scattering amplitude A_S that is independent of r and z is expressed as

$$A_S(\theta) = \frac{\mathrm{i}\omega}{g\pi}\sum_{m=0}^{\infty}(-\mathrm{i})^m A_m\cos(m\theta). \tag{11}$$

Resonance within the annular metamaterial ring.–Analogous to the gap resonance by two side-by-side barges [3], we impose the homogeneous Dirichlet-type condition at open ends of the channel ends giving rise to

$$\begin{cases} C_m J_0(kR_\mathrm{i}) + D_m Y_0(kR_\mathrm{i}) = 0, \\ C_m J_0(kR) + D_m Y_0(kR) = 0. \end{cases} \tag{12}$$

The condition that the above equation system has nontrivial solutions requires

$$J_0(k_j R_\mathrm{i})Y_0(k_j R) - J_0(k_j R)Y_0(k_j R_\mathrm{i}) = 0, \tag{13}$$

where $k_j \in \mathbb{R}^+$ for $j = 1, 2, 3, \cdots$ denotes the jth root, which is associated to the jth resonant frequency. If we substitute the large-argument asymptotic forms of Bessel functions and Neumann functions, we will get $k_j(R - R_\mathrm{i}) \approx j\pi$, which is in line with the Fabry-Pérot resonance condition [4]. For $R_\mathrm{i}/R = 0.5$, the first three resonance frequencies correspond to $kR = 6.246, 12.547, 18.836$.

Broadband near non-back-scattering.–We demonstrate that there can be hardly any back scattering for a wide range of wave frequencies (see Fig. 1). The near non-back-scattering generally happens around the predicted resonant frequencies. There are a series of spikes observed on the curves of $|A_S|/A - kR$ at the non-resonant wave conditions around $kR = 4.0$, 9.0, and 16.0. The forward-scattering coefficient $|A_S(0)|/A$ presents an overall step-shaped growth with the increase of kR. The three resonant frequencies in the computed range of wave conditions

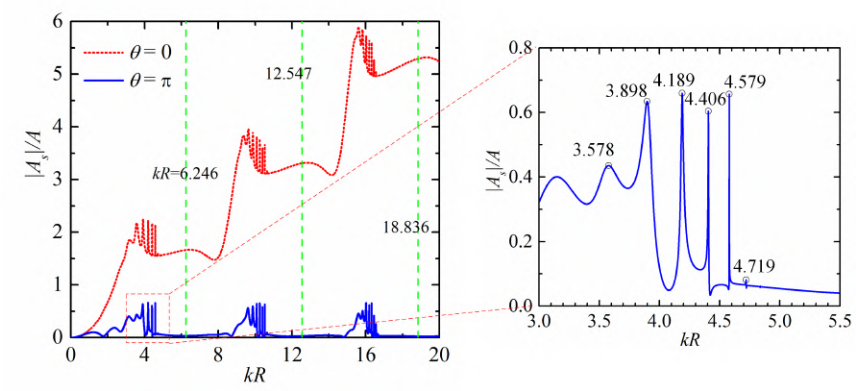

Figure 1: Frequency response of the far-field scattering coefficient in terms of $|A_S|/A$ at $\theta = 0$ and π, $R/h = 1.0$, $R_\mathrm{i}/R = 0.5$. The green dash lines represent the positions of the resonant frequencies.

and four other wave frequencies associated to the peaks of the curve of $|A_S(\pi)|/A - kR$ around $kR = 4.0$ are selected to be examined in details that follow.

The near-field wave fields in terms of the wave amplitude and the instantaneous wave response at $t = 0$ for the three resonant frequencies and the four none-resonant frequencies are plotted in Figs. 2 and 3, respectively. An excellent agreement between the numerical and analytical results are obtained (Figs. 2a vs. 2b), giving confidence in the present analytical model for solving water scattering problem by an annular metamaterial cylinder.

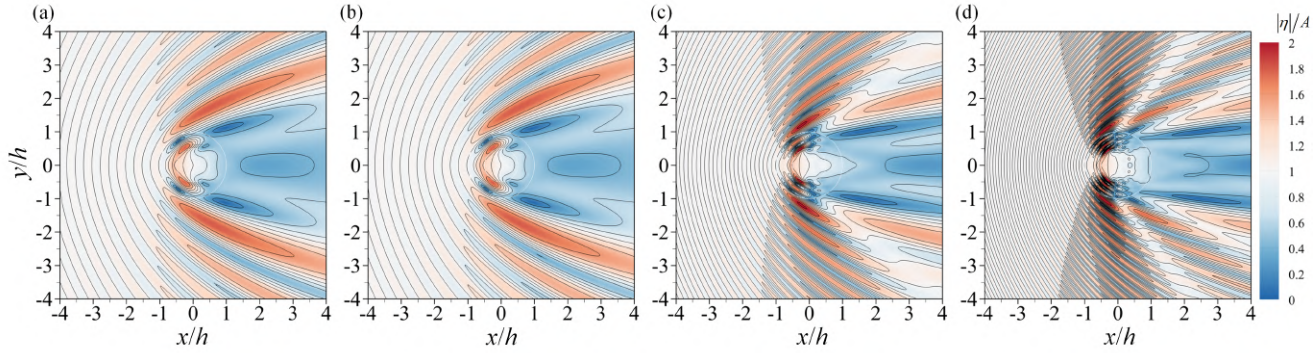

Figure 2: The maximum free surface amplitude, $R/h = 1.0$, $R_\mathrm{i}/R = 0.5$: (a) numerical results [2]; (b)-(d) analytical results. (a)-(b) $kR = 6.246$; (c) $kR = 12.547$; (d) $kR = 18.836$. For the numerical results, the annular metamaterial cylinder is composed of 128 infinitely-thin vertical plates aligned with the radial direction and uniformly distributed all over the angular direction.

For the resonant wave frequencies, the waves are attenuated after passing through the annular metamaterial cylinder because of the fluid-structure interaction. The larger the incident wavelength, the wider the 'open angle' of the attenuated domain at the lee side of the annular metamaterial cylinder. The diffracted waves are generated at the front-side half-ring of the annular metamaterial cylinder and, taking that as a centre, propagate outwards in all directions. The diffracted waves are perfectly transmitted through each small channel with no phase delay. For the jth resonant frequency, which satisfies $k_j(R - R_\mathrm{i}) \approx j\pi$, i.e., the length of each channel is $j/2$ times as large as the wavelength, j regions of large amplitude of the diffracted waves are generated and developed at the channels over $\theta \in (0.5\pi, \pi)$, and ultimately travel outwards in the open sea with different propagating directions. The waves are found to travel in curved paths in the metamaterial annular domain. When the waves cross the boundary between the metamaterial region and the exterior open sea, there is a sudden change in propagating direction, resulting in 'wave refraction'. For the non-resonant wave frequencies, there is a phase delay when diffracted waves are transmitted through each small channel, showing an 'impedance effect'. A 'sloshing' type motion of the diffracted waves along the x-axis is observed at the annular domain. Consequently, the diffracted waves are generated all over the annular metamaterial cylinder and, taking the out edge as a series of sources, propagate outwards.

Non-scattering at the center point.–We observe that the amplitude of the wave response at $r = 0$ is 1.0 regardless of the wave frequencies, e.g., see Fig. 2-3. This can be theoretically explained and approved with our model. Since $J_0(0) = 1.0$ and $J_m(0) = 0$ for $m > 0$, the wave response at $r = 0$ reads $\eta(0, \theta) = \mathrm{i}\omega B_0/g$. In the present model, we have $B_0 = -\mathrm{i}gA/\omega$, which gives $\eta(0, \theta) = A$. This means the wave motion at the center of the annular metamaterial cylinder is identical to the incident waves in terms of both amplitude and phase, i.e.,

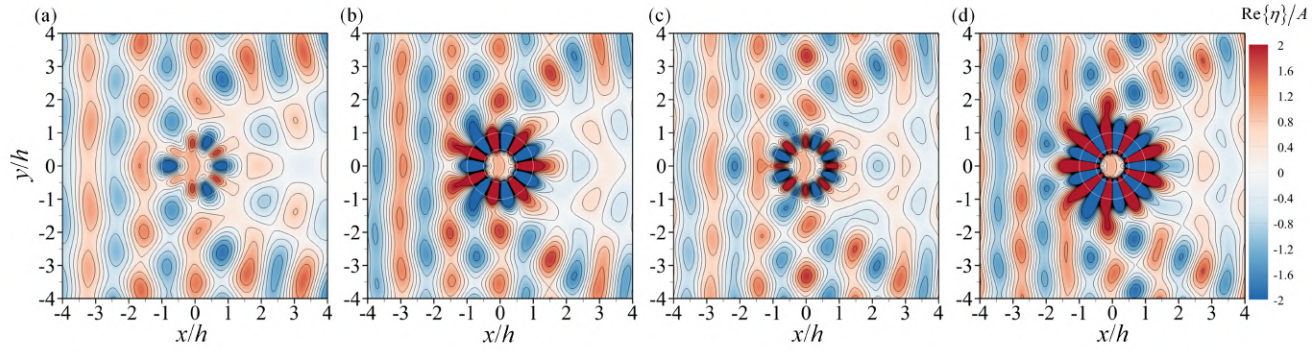

Figure 3: The instantaneous free surface at $t = 0$, $R/h = 1.0$, $R_i/R = 0.5$: (a) $kR = 3.898$; (b) $kR = 4.189$; (c) $kR = 4.406$; (d) $kR = 4.579$.

non-scattering at the center point.

Wave near-trapping.–By allowing k to become complex we can consider solutions which represent localised wave oscillations that exist in the absence of incident wave forcing. Such modes are defined by solutions to

$$f(n,k) = \det \mathbf{A}(n,k) = 0, \tag{14}$$

where $\mathbf{A}(n,k)$ denotes the coefficient matrix in Eq. (9). Figure 4 shows the roots of $f(n,k) = 0$ in the complex kR plane. The roots for $n = 5 \sim 10$ close to the real axis around $kR = 4.0$ are $3.557 - 0.108$i, $3.909 - 0.038$i, $4.188 - 0.010$i, $4.406 - 0.002$i, $4.579 - 2.7 \times 10^{-4}$i, and $4.720 - 3.0 \times 10^{-5}$i, respectively. It is clear that the first cluster of the spikes of the response as shown in Fig. 1 can be associated with these roots, i.e., the spikes at frequencies corresponding to near-trapping are related to the near-vanishing of the determinant.

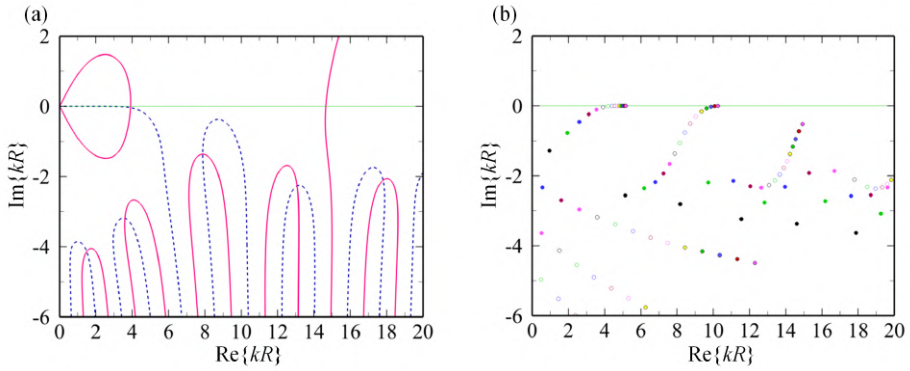

Figure 4: Wave near-trapping for $R/h = 1.0$, $R_i/R = 0.5$: (a) Location of the roots of $f(n,k) = 0$ in the complex kR plane for $n = 6$. The blue dashed lines identify the contours $\mathrm{Re}\{f(n,k)\} = 0$, whereas the pink solid lines correspond to the contours $\mathrm{Im}\{f(n,k)\} = 0$; (b) Location of zeros of determinant as n varies from 1 to 15.

The research was supported by Open Research Fund Program of State Key Laboratory of Hydroscience and Engineering (Tsinghua University) [grant number sklhse-2021-E-02]. R.P. acknowledges support from the EPSRC [grant number EP/V04740X/1]. D.G. gratefully acknowledges the EPSRC for supporting part of this work through the Supergen ORE Hub, EP/S000747/1.

References

[1] A. U. Jan and R Porter. Transmission and absorption in a waveguide with a metamaterial cavity. *The Journal of the Acoustical Society of America*, 144(6):3172–3180, 2018.

[2] H. Liang, S. Zheng, Y. Shao, K. H. Chua, Y. S. Choo, and D. Greaves. Water wave scattering by impermeable and perforated plates. *Phys. Fluids*, 33(7):077111, 2021.

[3] B. Molin. On the piston and sloshing modes in moonpools. *J. Fluid Mech.*, 430:27–50, 2001.

[4] M. M. Sadeghi, Sucheng Li, Lin Xu, Bo Hou, and Huanyang Chen. Transformation optics with Fabry-Pérot resonances. *Sci. Rep.*, 5:8680, 2015.

[5] S. Zheng, R. Porter, and D. Greaves. Wave scattering by an array of metamaterial cylinders. *J. Fluid Mech.*, 903:A50, 2020.